Structure, Magnetism, and Colossal Magnetoresistance (CMR) of the Ternary Transition Metal Solid Solution $Ca_{14-x}Eu_xMnSb_{11}$ ($0 < x < 14$)

Hyungrak Kim,[†,‡] Marilyn M. Olmstead,[†] Peter Klavins,[§] David J. Webb,[§] and Susan M. Kauzlarich*[,†]

Departments of Chemistry and Physics, University of California, One Shields Avenue, Davis, California 95616

Received February 1, 2002. Revised Manuscript Received May 23, 2002

The solid solution of the ternary transition metal Zintl phase $Ca_{14-x}Eu_xMnSb_{11}$ ($0 < x < 14$) has been prepared by heating a mixture of stoichiometric amounts of the elements in a two-zone furnace with $T_{high} = 1100$ °C and $T_{low} = 1050$ °C. The ternary transition metal compounds crystallize in the tetragonal space group $I4_1/acd$ and are isostructural with the Zintl compound $Ca_{14}AlSb_{11}$. The lattice parameters of the $Ca_{14-x}Eu_xMnSb_{11}$ compounds linearly increase with increasing Eu substitution for Ca. The Eu atoms preferentially occupy the Ca(2) site first and subsequently occupy Ca(4), Ca(1), and Ca(3), in order, among the four crystallographically inequivalent Ca sites. Temperature-dependent magnetic susceptibility measurements of the solid solution reveal that Eu replacement for Ca induces complex magnetic interactions in the compound, from simple ferromagnetic interactions for $Ca_{14}MnSb_{11}$ to ferrimagnetic interactions for $Eu_{14}MnSb_{11}$, because of the $Eu^{2+}(4f^7)$ magnetic moment. The paramagnetic Curie temperature of the $Ca_{14-x}Eu_xMnSb_{11}$ compounds shows an interesting change with varying x, and the magnetic easy axis gradually changes in the solid solution from perpendicular (for $Ca_{14}MnSb_{11}$) to parallel (for $Eu_{14}MnSb_{11}$) to the crystal c axis. The electrical transport properties of the $Ca_{14-x}Eu_xMnSb_{11}$ ($x = 0$, 3, 11) compounds show a close relation to their magnetic properties and are compared to the previous results for $Ca_{14-x}Eu_xMnSb_{11}$ ($x = 13$, 14). The influence of Eu doping on the structural and physical property of $Ca_{14-x}Eu_xMnSb_{11}$ is discussed in terms of the site preferences of Eu for the four different Ca sites.

Introduction

Recent doping studies of the compounds $Eu_{14-x}A_xMnSb_{11}$ ($x < 3$, A = Ca, Sr, Ba, or Yb),[1,2] targeting a better understanding of the negative colossal magnetoresistance (CMR) effect of $Eu_{14}MnSb_{11}$, have shown that the complicated magnetic interactions between 3d and 4f electrons in the ternary rare earth transition metal Zintl phase could be probed by the substitution of magnetically inactive elements into the magnetic Eu sites. In particular, the site preference of each dopant, depending on its ionic radius, for the four Eu sites in the crystal structure provides key information about the different contributions of the Eu sites to the bulk magnetic and magnetotransport properties and elucidate the close structure−property relationship in this compound. We have suggested that the increase of the ferromagnetic transition temperature of $Eu_{14}MnSb_{11}$,[3] compared to those of the alkaline earth analogues such as $Ca_{14}MnSb_{11}$,[4] results from the unique combination of itinerant 3d electrons with the localized 4f electrons. A small amount of Eu replacement by alkaline earth dopants changes every feature of the intriguing magnetic behavior of the compound caused by three different types[5−8] of magnetic interactions in the ternary rare earth transition metal compound: the R−R interaction (4f−4f), the R−T interaction (4f−3d), and the T−T interaction (3d−3d).

The $A_{14}MnPn_{11}$ (A = divalent cation, Pn = pnictogen element) family of compounds[9] is isostructural to $Ca_{14}AlSb_{11}$,[10] and the crystal structure of the compound can be understood by utilizing the well-known Zintl−Klemm

* To whom correspondence should be addressed. Phone: (530)752−4756. Fax: (530)752-8995. E-mail: smkauzlarich@ucdavis.edu.
† Department of Chemistry.
‡ Present address: C-PCS, Los Alamos National Laboratory.
§ Department of Physics.

(1) Kim, H.; Klavins, P.; Kauzlarich, S. M. *Chem. Mater.* **2002**, *14*, 2308−2316.
(2) Kim, H.; Chan, J. Y.; Olmstead, M. M.; Klavins, P.; Webb, D. J.; Kauzlarich, S. M. *Chem. Mater.* **2002**, *14*, 206−216.
(3) Chan, J. Y.; Wang, M. E.; Rehr, A.; Kauzlarich, S. M.; Webb, D. J. *Chem. Mater.* **1997**, *9*, 2132−2138.
(4) Rehr, A.; Kuromoto, T. Y.; Kauzlarich, S. M.; Castillo, J. D.; Webb, D. J. *Chem. Mater.* **1994**, *6*, 93−99.
(5) Buschow, K. H. J. *Ferromagnetic Materials*; Wohlfarth, E. P., Ed.; North-Holland Publishing Company: Amsterdam, 1980; Vol. 1, pp 297−414.
(6) Li, H. S.; Coey, J. M. D. In *Handbook of Magnetic Materials*; Buschow, K. H. J., Ed.; Elsevier Science Publishers B.V.: Amsterdam, 1991; Vol. 6, pp 1−83.
(7) Szytula, A. In *Handbook of Magnetic Materials*; Buschow, K. H. J., Ed.; Elsevier Science Publishers B.V.: Amsterdam, 1991; Vol. 6, pp 85−180.
(8) Wallace, W. E. *Rare Earth Intermetallics*; Academic Press: New York, 1973.
(9) Kauzlarich, S. M. In *Chemistry, Structure, and Bonding of Zintl Phases and Ions*; Kauzlarich, S. M., Ed.; VCH Publishers: New York, 1996; pp 245−274.

10.1021/cm020065w CCC: $22.00
Published on Web 07/11/2002

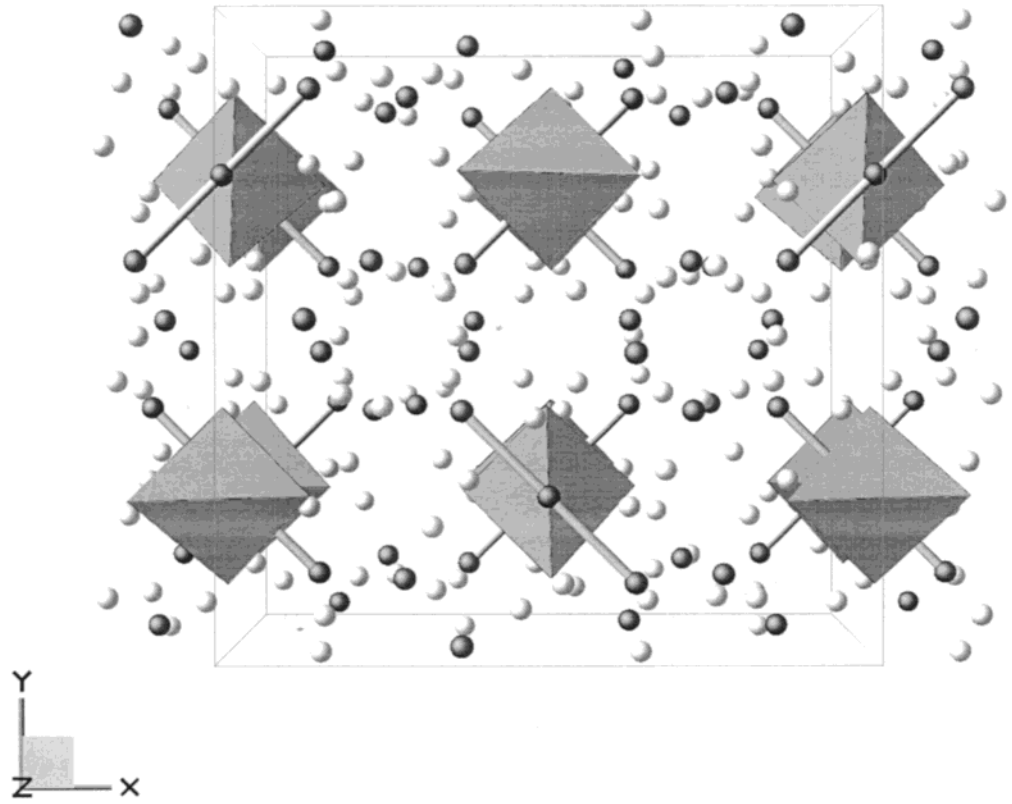

Figure 1. Perspective view down the *z* axis of the unit cell of $Ca_{14}AlSb_{11}$. Gray polyhedra, $AlSb_4$; white circles, Ca; black circles, Sb.

concept.[11,12] Figure 1 shows a perspective view of the unit cell along the *c* axis of $Ca_{14}AlSb_{11}$. $Ca_{14}AlSb_{11}$ crystallizes in a body-centered tetragonal unit cell in the space group $I4_1/acd$ with eight formula units (208 atoms). A formula unit consists of 14 Ca^{2+} cations, 4 isolated Sb^{3-} ions, a distorted $AlSb_4^{9-}$ tetrahedron, and a Sb_3^{7-} linear anion. The magnetic property of this family of compounds has been described within the Ruderman−Kittel−Kasuya−Yosida (RKKY) theory,[13−15] where the Mn−Mn distances and the presence of the rare earth magnetic moments are important in raising the ferromagnetic transition temperature T_C.[16]

Because the large unit cell has prohibited a plausible theoretical calculation of the electronic structure of $Eu_{14}MnSb_{11}$, the solid solution study seems to be a good alternative for gaining insight into the role of Eu in the magnetic and electronic properties of the compound. In the present study, we have inverted our previous approaches[1,2] of Eu site doping with magnetically inactive dipositive metal cations in $Eu_{14}MnSb_{11}$ to Eu doping into the Ca sites in $Ca_{14}MnSb_{11}$. $Ca_{14}MnSb_{11}$ has been chosen because it is relatively less air-sensitive and has the highest transition temperature among the alkaline earth analogues with the $Ca_{14}AlSb_{11}$ structure. In this way, we are starting with a relatively simpler system; plotting the physical properties as a function of increasing Eu concentration might be easier to correlate to the influence of Eu 4f electrons in the compound rather than using the opposite approach, with doping Ca into $Eu_{14}MnSb_{11}$.

The whole range of solid solution between the two end compounds, $Eu_{14}MnSb_{11}$ and $Ca_{14}MnSb_{11}$, has been synthesized in single-crystal and polycrystalline form using the same methods as described in our previous studies.[1,2] Changes in various physical property, including structural parameters and magnetic behaviors, are discussed as a function of Eu doping concentration in this paper. Although we should not expect a significant change in the electronic band structure because of the divalency of both Eu and Ca, the electrical properties of $Ca_{14-x}Eu_xMnSb_{11}$ can be monitored from resistivity measurements.

Experimental Section

Synthesis. Eu metal was obtained from Ames Lab (99.999%) and cut into small pieces. Ca pieces (J. Matthey, 99.99%) and Sb metal (J. Matthey, 99.9999%) were used as received. Mn flakes (J. Matthey, 99.98%) were first cleaned in a 5% HNO_3/CH_3OH solution, transferred into a drybox, and ground into a powder. All materials were handled in a nitrogen-filled drybox. All of the $Ca_{14-x}Eu_xMnSb_{11}$ samples were prepared by weighing stoichiometric amounts of the elements in a drybox, loading them into a clean tantalum tube with a sealed end, and subsequently sealing the tube in an argon-filled arc welder. Ta tubes had been cleaned prior to arc welding with a 20% HF, 25% HNO_3, and 55% H_2SO_4 solution. The sealed Ta tube was further sealed in a fused silica tube under 0.2 atm of purified argon. Reflective polycrystalline pieces and single-crystal needles (1−2 mm) were obtained by heating the mixtures in a two-zone furnace with T_{high} = 1100 °C and T_{low} = 1050 °C for 10 days, followed by furnace cooling. All reaction

(10) Cordier, G.; Schäfer, H.; Stelter, M. *Z. Anorg. Allg. Chem.* **1984**, *519*, 183−188.
(11) Zintl, E. *Angew. Chem.* **1939**, *52*, 1.
(12) Klemm, W. *Proc. Chem. Soc. London* **1958**, 329.
(13) Ruderman, M. A. *Phys. Rev.* **1954**, *96*, 99−102.
(14) Kasuya, T. *Prog. Theor. Phys.* **1956**, *16*, 45−57.
(15) Yosida, K. *Phys. Rev.* **1957**, *106*, 893−898.
(16) Chan, J. Y.; Kauzlarich, S. M.; Klavins, P.; Liu, J.-Z.; Shelton, R. N.; Webb, D. J. *Phys. Rev. B* **2000**, *61*, 459−463.

Table 1. Lattice Parameters of the $Ca_{14-x}Eu_xMnSb_{11}$ Solid Solution

compound	x^a	a (Å)	c (Å)	a/c	V (Å^3)
$Ca_{14}MnSb_{11}$	0.0	16.7495(6)	22.1116(8)	0.7575	6203.3(4)
$Ca_{12.66}Eu_{1.34}MnSb_{11}$	1.34(1)	16.7963(6)	22.1567(8)	0.7581	6250.8(4)
$Ca_{10.74}Eu_{3.26}MnSb_{11}$	3.26(1)	16.8685(8)	22.1974(10)	0.7599	6316.2(5)
$Ca_{9.39}Eu_{4.61}MnSb_{11}$	4.61(1)	16.9297(7)	22.2492(9)	0.7609	6377.0(5)
$Ca_{7.18}Eu_{6.82}MnSb_{11}$	6.82(1)	17.014(9)	22.2998(12)	0.7630	6455.3(6)
$Ca_{5.35}Eu_{8.65}MnSb_{11}$	8.65(1)	17.0832(8)	22.4131(10)	0.7622	6540.9(5)
$Ca_{2.81}Eu_{11.19}MnSb_{11}$	11.19(1)	17.1737(7)	22.5741(10)	0.7608	6657.9(5)
$Ca_{1.47}Eu_{12.53}MnSb_{11}$	12.53(1)	17.2235(7)	22.6555(9)	0.7602	6720.7(5)
$Eu_{14}MnSb_{11}$	14.0	17.2973(6)	22.7499(9)	0.7603	6806.7(4)

[a] From the refinement of single-crystal X-ray diffraction data.

tubes were opened and examined in a nitrogen-filled drybox equipped with a microscope at water levels of less than 1 ppm.

Structure Determination. Highly reflective needle crystals from the reactions were transferred to Exxon Paratone N oil for X-ray structure determination. A suitable crystal was mounted on a thin glass fiber and positioned under a cold stream of N_2 in a Bruker SMART 1000 CCD diffractometer equipped with a CRYO cooler low-temperature apparatus (CRYO Industries of America, Inc.). No decomposition of the crystal was observed during data collection (inferred from the intensity of 50 remeasured frames). The SMART software[17] was used for data collection, and SAINT[18] was used for data integration. The absorption correction was performed using SADABS. The structure was solved by direct methods and refined using SHELXL-97.[19] Data collection parameters and crystallographic data are provided in Table 1. Detailed crystallographic data and anisotropic thermal parameters are provided as Supporting Information. X-ray powder diffraction data of the products were obtained using an Enraf-Nonius Guinier camera equipped with a quartz monochromator to yield Cu $K\alpha_1$ radiation. Powdered silicon (NBS) was included in the samples as an internal standard.

Magnetic Susceptibility and Transport Measurements. DC magnetization data were obtained with a Quantum Design MPMS superconducting quantum interference device (SQUID) magnetometer with a 7-T superconducting magnet. The data were collected and analyzed with the Quantum Design Magnetic Property Measurement System (MPMS) MultiVu software.[20] For single-crystal magnetic measurements, the same crystal that was used for the structure determination was mounted in a sample holder for measurement. Powdered samples were prepared in a drybox by loading 30−50 mg of powder into a gelatin capsule and placing the capsule into a sample holder. Magnetoresistance measurements of the $Ca_{14-x}Eu_xMnSb_{11}$ (x = 0, 3, 11, 13) compounds were performed on needle-shaped single crystals using a standard four-probe method. A constant current (0.1 mA) was applied to the sample along the crystal c axis through the two outer leads (Keithley model 224 current source), and the voltage was measured across the two inner leads (Keithley model 181 nanovoltmeter).

Results and Discussion

Structure. The crystal structures of the doped system were first refined as $Ca_{14}MnSb_{11}$, and then Eu was substituted into the various Ca sites by examining the thermal parameters. The models presented in this paper provides the lowest R values and most reasonable thermal parameters in the refinements. All of the $Ca_{14-x}Eu_xMnSb_{11}$ (x = 0−14) compounds are isostructural to $Ca_{14}AlSb_{11}$,[10] and this structure type has been described in detail previously.[4,9,10,21,22] The crystal structure is characterized by alternating $AlSb_4^{9-}$ tetrahedra and linear Sb_3^{7-} anions along the crystallographic c axis as shown in Figure 1. All of the Mn sites are crystallographically equivalent and approximately 10 Å apart from their nearest neighbors, and there are four crystallographically inequivalent Ca and Sb sites in the crystal structure.

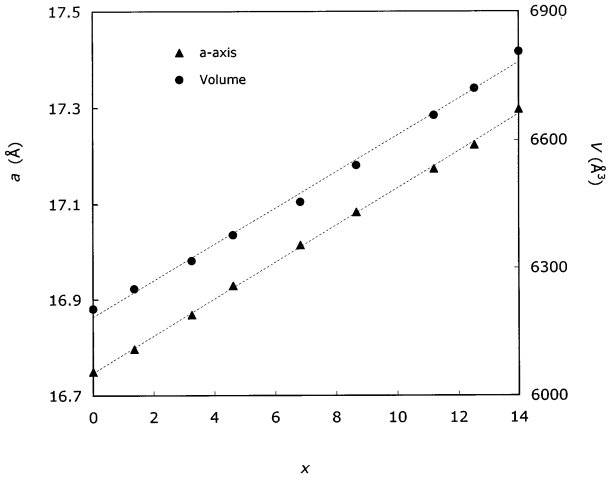

Figure 2. Lattice parameter changes as a function of Eu doping amount in $Ca_{14-x}Eu_xMnSb_{11}$ single crystals. The lines are guides for the eye.

The unit cell parameters of the $Ca_{14-x}Eu_xMnSb_{11}$ ($0 < x < 14$) compounds increase with increasing x, as reported in Table 1, and they are plotted as a function of x in Figure 2. The linear change of the lattice parameters is consistent with Vegard's law and indicates that this system should be a solid solution. The increase of the lattice parameters with increasing amount of Eu substitution for Ca is attributed to the larger ionic radius of Eu^{2+} (1.31 Å) compared to that of Ca^{2+} (1.14 Å)[23] as observed in the previous doping studies[1,2] on $Eu_{14}MnSb_{11}$. Variations of the cell parameter ratio between the a and c axes are very small, less than 1%, throughout the whole range of the solid solution, as shown in Table 1.

Table 2 provides the refinement results of the fractional site occupancies of the Eu and Ca ions in the four different A sites of the $A_{14}MnSb_{11}$ structure. There is a preference in Eu substitution into the four different unique crystallographic Ca sites, and the trend is followed throughout the range of the solid solution, as

(17) *SMART*; Siemens Analytical X-ray Systems, Inc.: Madison, WI, 1994.
(18) *SAINT*, 6th ed.; Siemens Analytical X-ray Systems, Inc.: Madison, WI, 1999.
(19) Sheldrick, G. M. *SHELXTL*, version 5.10; Bruker AXS, Inc.: Madison, WI, 1997.
(20) *MPMS XL-7 with MultiVu Software*; Quantum Design, Inc.: San Diego, CA.
(21) Kuromoto, T. Y.; Kauzlarich, S. M.; Webb, D. J. *Chem. Mater.* **1992**, *4*, 435−440.
(22) Rehr, A.; Kauzlarich, S. M. *J. Alloys Compd.* **1994**, *207/208*, 424−426.
(23) Shannon, R. D. *Acta Crystallogr.* **1976**, *A32*, 751.

Table 2. Fractional Site Occupancies (%) of Eu the Four Crystallographically Inequivalent Ca Sites

compound	x^a	Ca(1)	Eu(1)	Ca(2)	Eu(2)	Ca(3)	Eu(3)	Ca(4)	Eu(4)
$Ca_{14}MnSb_{11}$	0.0	100.0	0.0	100.0	0.0	100.0	0.0	100.0	0.0
$Ca_{12.66}Eu_{1.34}MnSb_{11}$	1.34(1)	97.4	2.6(2)	77.9	22.1(2)	98.6	1.4(3)	92.0	8.0(2)
$Ca_{10.74}Eu_{3.26}MnSb_{11}$	3.26(1)	91.4	8.6(3)	51.9	48.1(3)	95.0	5.0(4)	77.8	22.2(3)
$Ca_{9.39}Eu_{4.61}MnSb_{11}$	4.61(1)	83.1	16.9(3)	40.4	59.6(3)	90.8	9.2(4)	65.7	34.3(3)
$Ca_{7.18}Eu_{6.82}MnSb_{11}$	6.82(1)	68.3	31.7(3)	24.0	76.0(3)	81.2	18.8(5)	46.6	53.4(3)
$Ca_{5.35}Eu_{8.65}MnSb_{11}$	8.65(1)	52.8	47.2(3)	15.5	84.5(3)	67.5	32.5(4)	31.6	68.4(3)
$Ca_{2.81}Eu_{11.19}MnSb_{11}$	11.19(1)	28.0	72.0(3)	7.5	92.5(3)	40.0	60.0(4)	14.8	85.2(3)
$Ca_{1.47}Eu_{12.53}MnSb_{11}$	12.53(1)	14.2	85.8(3)	4.5	95.5(3)	21.2	78.8(4)	7.5	92.5(3)
$Eu_{14}MnSb_{11}$	14.0	0.0	100.0	0.0	100.0	0.0	100.0	0.0	100.0

[a] From the refinement of single-crystal X-ray diffraction data.

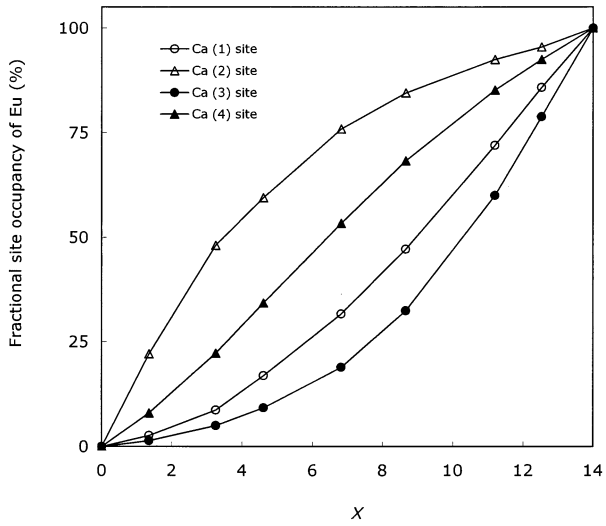

Figure 3. Fractional site occupancies of Eu in the four crystallographically inequivalent Ca sites.

plotted in Figure 3. The Eu atoms preferentially occupy the Ca(2) site first and, subsequently, the Ca(4), Ca(1), and Ca(3) sites, in that order. The Eu replacement in the Ca(2) site becomes as high as 50% with only 23% Eu doping overall ($x = 3.3$ in $Ca_{14-x}Eu_xMnSb_{11}$), whereas the Eu replacement in the Ca(3) site reaches more than 50% with approximately 80% Eu doping overall ($x = 11.2$ in $Ca_{14-x}Eu_xMnSb_{11}$). This site preference can be explained by considering the structural environment of the four Ca sites. In brief, the larger Eu atoms prefer to substitute for the Ca atoms in the more spacious and distorted Ca(2) site, rather than the sterically restricted and highly symmetric Ca(3) site, therefore providing less structural perturbation.

The site preference of Eu plays an important role in explaining the magnetic behavior of the $Ca_{14-x}Eu_xMnSb_{11}$ solid solution. It allows us to determine the contribution of each A metal site to the bulk magnetic property of the compounds. A detailed discussion concerning the relationship between the Eu site preference and magnetic properties is presented in the next section.

Magnetism. Figure 4 shows the temperature-dependent magnetization of single-crystal samples of the $Ca_{14-x}Eu_xMnSb_{11}$ solid solution in an applied field of 1000 Oe. The two end compounds, i.e., $Eu_{14}MnSb_{11}$ and $Ca_{14}MnSb_{11}$, were synthesized under the same conditions as the mixed systems, and their data have been added for comparison. For each sample, the needle-shaped crystal was placed with its long crystal *c* axis parallel (●) to the applied field and then rotated perpendicular (×) to the applied field to determine the magnetocrystalline anisotropy in the compound.

The classical ferromagnetic behavior observed in $Ca_{14}MnSb_{11}$ disappears rapidly with small amounts of Eu substitution into the Ca sites in $Ca_{12}Eu_2MnSb_{11}$ as shown in Figure 4b, indicating the strong influence of the A(2) site on the magnetic properties of $A_{14}MnSb_{11}$ compounds. It is noteworthy that small amounts of Ca doping in the Eu sites, mainly the Eu(3) site, do not cause any large changes in the magnetization of the doped $Eu_{14-x}Ca_xMnSb_{11}$ ($x < 3$) system.[2] As the Eu substitution increases, the magnetic easy axis of $Ca_{14-x}Eu_xMnSb_{11}$ changes from the crystallographic *a* or *b* axis to the *c* axis. The magnetic susceptibility of the compounds when the *c* axis is oriented parallel to the applied field is smaller than that obtained when the *c* axis is oriented perpendicular for $x \leq 7$ (Figure 4a−d). For $x \geq 9$, however, the susceptibility for the parallel direction of the solid solutions is larger than that for the perpendicular direction (Figure 4e−h). The onset of antiferromagnetic ordering caused by a Eu−Eu magnetic interaction is observed for $x \geq 11$ in $Ca_{14-x}Eu_xMnSb_{11}$, and this ordering temperature increases as the amount of Eu substitution increases. The low-temperature upturn in the magnetization of $Ca_{14-x}Eu_xMnSb_{11}$ ($x \geq 11$) oriented perpendicular to the applied field was discussed in detail in the previous $Eu_{14-x}Ca_xMnSb_{11}$ ($x < 3$) study.[2]

Finally, the temperature-dependent magnetization of $Eu_{14}MnSb_{11}$ oriented parallel to the applied field in Figure 4h can be explained as the stepwise occurrence of three different magnetic interactions in the ternary rare earth transition metal compound: the T−T interaction (3d−3d), the R−T interaction (4f−3d), and the R−R interaction (4f−4f). As the temperature decreases, the compound exhibits a ferromagnetic transition first, then a canted ferromagnetic state, and at the lowest temperature, a pure antiferromagnetic state. This feature in the magnetization is reminiscent of the magnetization study of the $URu_{0.4}Pd_{0.6}Ga$ system[24] and is explained by the same stepwise occurrence of magnetic orderings.

The field-dependent magnetization curves of the single-crystal samples of the $Ca_{14-x}Eu_xMnSb_{11}$ solid solution at 5 K are plotted in Figure 5. Consistent with the temperature-dependent magnetization data shown in Figure 4, there is a change of the magnetic easy axis when $x = 9$. The high-field measurement shows that magnetization with different orientations approach the same saturation value. It is worthwhile mentioning that there is a metamagnetic transition in the Eu-rich phase of $Ca_{14-x}Eu_xMnSb_{11}$ ($x \geq 13$) oriented

(24) Tran, V. H.; Troc, R.; de V. du Plessis, O.; Andre, G.; Bouree, F. *Phys. Rev. B* **1997**, *56*, 11065−11072.

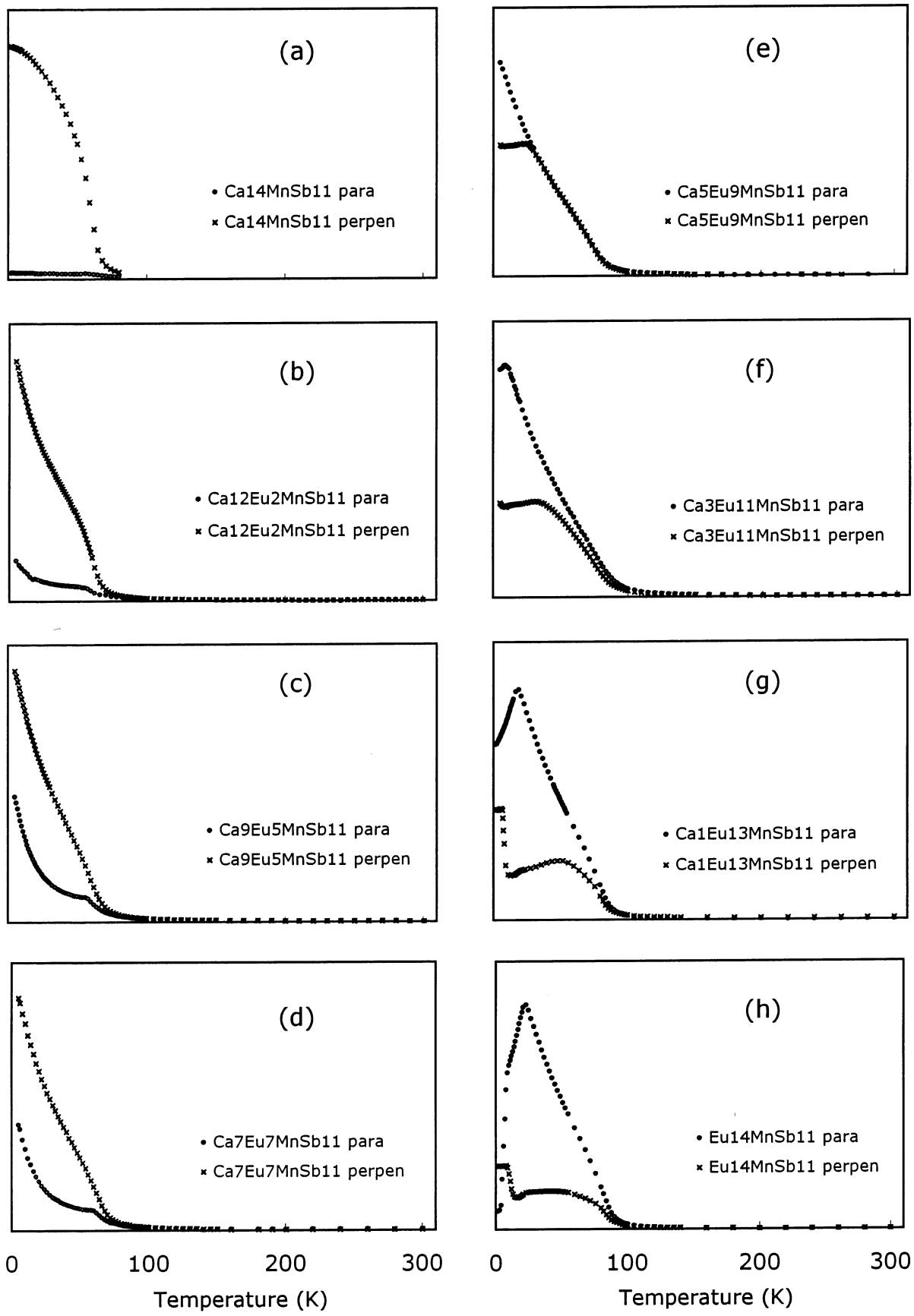

Figure 4. Temperature-dependent magnetization of single-crystal samples of $Ca_{14-x}Eu_xMnSb_{11}$ at an applied field 1000 Oe. (The *y* axis gives the magnetization in arbitrary units for comparison.)

parallel to the applied field, which is attributed to the onset of a pure antiferromagnetic phase at the lowest temperature.[2]

Magnetic property measurements were also performed on powder samples of the solid solution, and their magnetization results are plotted as a function of

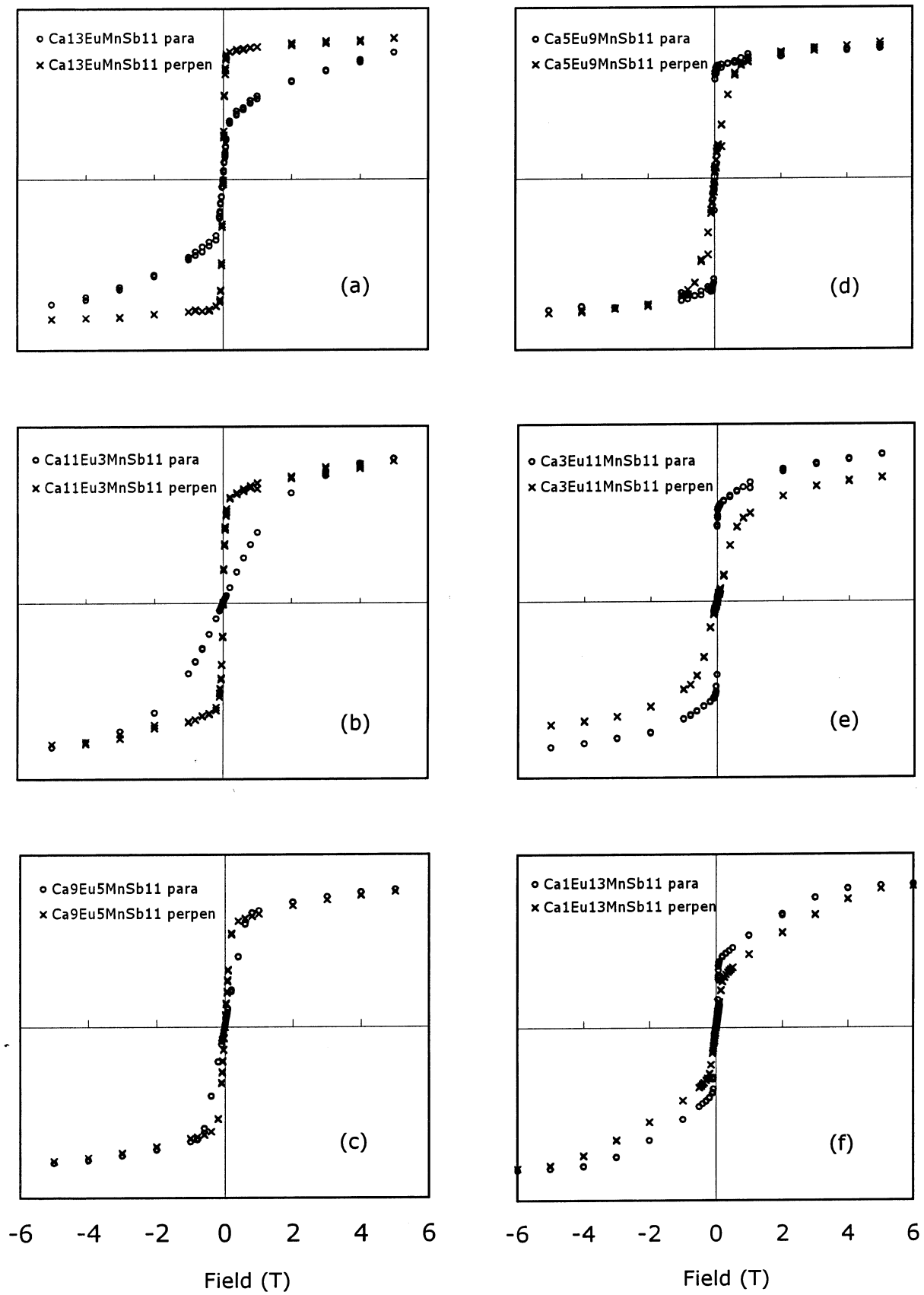

Figure 5. Hysteresis loop of single-crystal samples of $Ca_{14-x}Eu_xMnSb_{11}$ measured at 5 K. (The *y* axis gives the magnetization in arbitrary units for comparison.)

temperature in Figure 6. The inset shows inverse susceptibility as a function of temperature. The temperature-dependent magnetization of the randomly oriented powder samples exhibits good agreement with the results from the single-crystal samples shown in Figure 4, in terms of ordering temperature and onset of low-temperature antiferromagnetic ordering. The magnetic susceptibilities of the powder samples of the

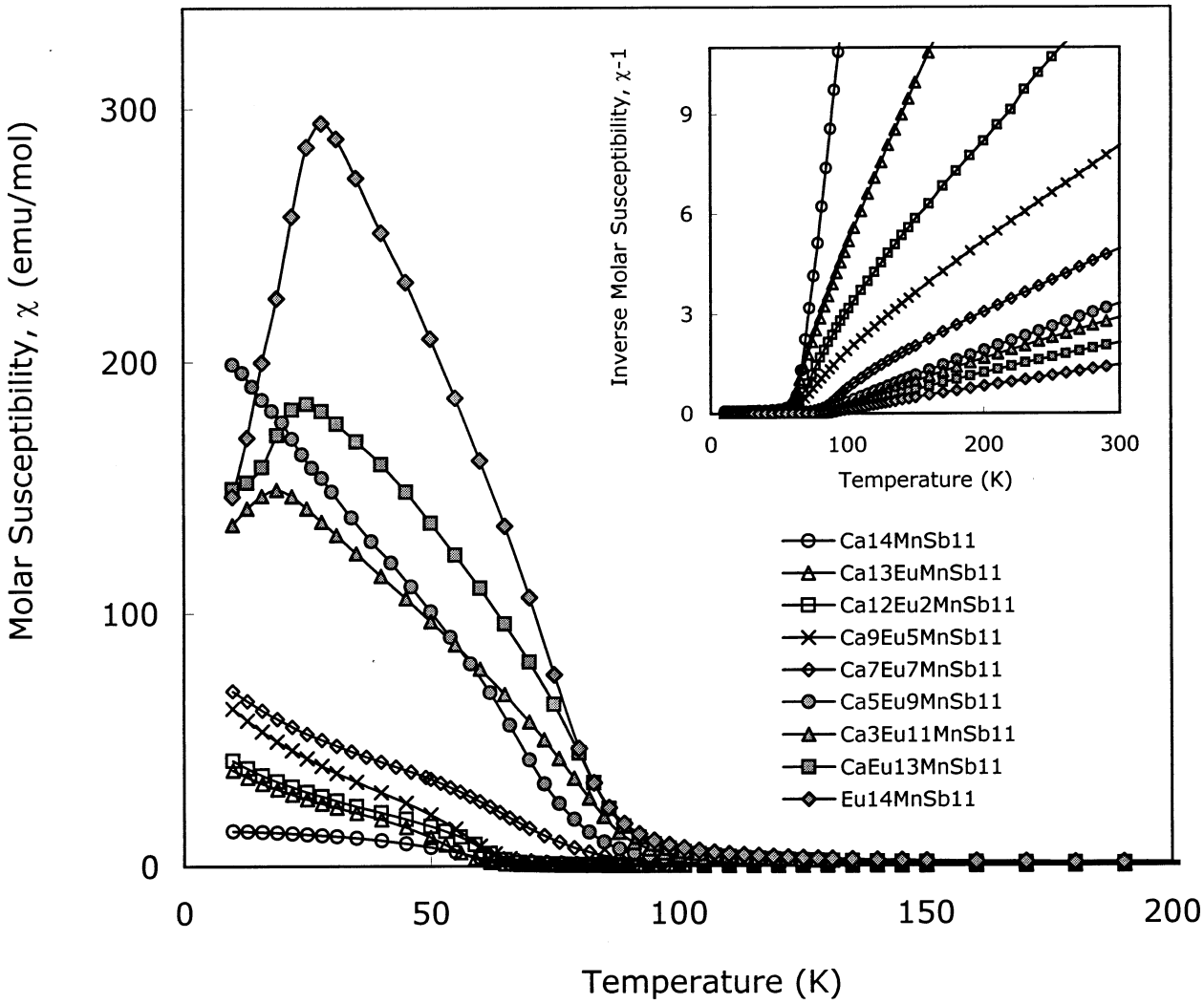

Figure 6. Temperature-dependent susceptibility of powder samples of $Ca_{14-x}Eu_xMnSb_{11}$. The inset shows the inverse susceptibility as a function of temperature.

Table 3. Magnetic Properties of $Ca_{14-x}Eu_xMnSb_{11}$ Compounds

compound	x	MW	χ_o[a]	C[a]	μ_{eff}[b] (μ_B)	μ_{cal}[c] (μ_B)	θ[a] (K)	T_C (K)	T_N (K)
$Ca_{14}MnSb_{11}$	0	1955	0.0022(5)	2.7(1)	4.7(1)	4.90	63.2(1)	64	–
$Ca_{13}EuMnSb_{11}$	1	2067	0.0054(4)	9.4(1)	8.7(1)	9.33	50.5(4)	56	–
$Ca_{12}Eu_2MnSb_{11}$	2	2179	0.016(1)	15.9(3)	11.3(2)	12.3	47.6(9)	59	–
$Ca_9Eu_5MnSb_{11}$	5	2515	0.030(1)	23.9(2)	13.8(1)	18.4	51.9(4)	60	–
$Ca_7Eu_7MnSb_{11}$	7	2738	0.0077(4)	30.5(6)	15.6(3)	21.6	74.4(5)	79	–
$Ca_5Eu_9MnSb_{11}$	9	2962	0.042(2)	57.5(2)	21.4(1)	24.3	79.5(1)	82	–
$Ca_3Eu_{11}MnSb_{11}$	11	3186	0.055(3)	62.0(2)	22.3(1)	26.8	85.2(1)	88	19.0
$Ca_2Eu_{12}MnSb_{11}$[d]	12	3298	−0.015(6)	71.0(5)	23.8(2)	27.9	86.4(1)	96	19.5
$CaEu_{13}MnSb_{11}$[d]	13	3410	0.0004(1)	90.6(7)	26.9(2)	29.0	84.9(1)	94	24.5
$Eu_{14}MnSb_{11}$	14	3522	0.068(6)	111.6(5)	29.9(1)	30.1	82.4(1)	91	28.0

[a] Obtained by fitting the data to the equation $\chi = \chi_o + C/(T - \theta)$. [b] Using the equation $\mu_{eff} = (8C)^{1/2}$. [c] Calculated for the Eu−Mn compound as $\mu_{cal}^2 = x\mu_{Eu}^2 + \mu_{Mn}^2$. [d] From ref 2.

$Ca_{14-x}Eu_xMnSb_{11}$ solid solutions below the transition temperature increase sharply with increasing x, indicating a significant influence of the Eu^{2+} ($4f^7$) ions on the bulk magnetic susceptibility. The ferromagnetic transition temperature of $Ca_{14-x}Eu_xMnSb_{11}$ also increases with increasing x. The increased magnetic susceptibility of the Eu-substituted compounds compared to that of $Ca_{14}MnSb_{11}$ is attributed to magnetic interactions between the rare earth and transition metals. We propose that the increase in the magnetic susceptibility and in the ferromagnetic transition temperature with increasing Eu content is due to enhanced magnetic interactions between transition metals, established with the help of surrounding Eu local 4f moments via intraatomic 5d polarization and subsequent interatomic Mn,3d−Eu,-5d exchange interactions.[25] These data are also consistent with a canted ferromagnetic or ferrimagnetic ordering between 3d and 4f magnetic sublattices, suggested from the previous doping studies.[1,2]

Table 3 provides results from fits of the high-temperature (100−300 K) susceptibility data of $Ca_{14-x}Eu_x$-$MnSb_{11}$ to a modified Curie−Weiss law. Analysis of the data in the paramagnetic regime illustrates that the effective magnetic moment of the solid solution in-

(25) Campbell, I. A. *J. Phys. F: Met. Phys.* **1972**, *2*, L47−50.

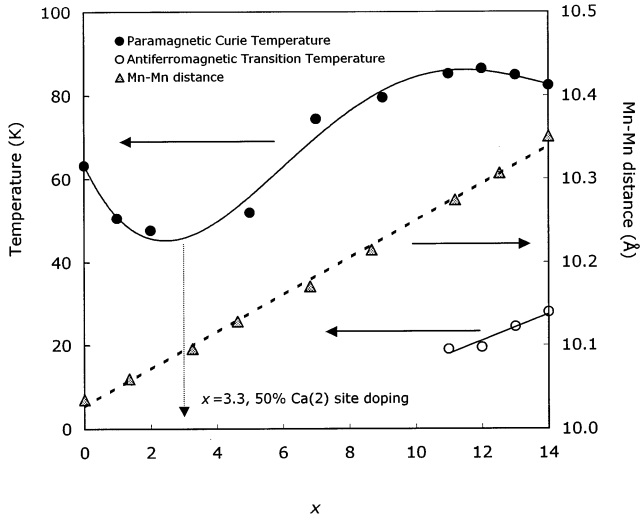

Figure 7. Paramagnetic Curie temperatures, antiferromagnetic transition temperatures, and Mn−Mn nearest-neighbor distances as a function of Eu concentration. The lines are guides for the eye.

creases as the magnetic Eu^{2+} ion substitution increases. The experimental magnetic moments for all compositions, except $x = 0$ and 1, are lower than the calculated values. The difference between the experimental magnetic moment and the calculated value has been attributed to two possible models:[2] a mixed valency (Eu^{2+}/Eu^{3+}) of Eu ions or an antiferromagnetic interaction between Eu−Eu and/or Eu−Mn. The trend of the paramagnetic Curie temperature (θ) and the ferromagnetic transition temperature (T_C) from Table 3 shows a very interesting change. The paramagnetic Curie temperature of $Ca_{14-x}Eu_xMnSb_{11}$ decreases until $x = 2$; then, it increases and reaches its maximum value at $x = 12$. It decreases again with the additional doping of Eu after $x = 12$. This behavior is depicted graphically in Figure 7, which shows the change in the paramagnetic Curie temperature and antiferromagnetic transition temperature as a function of doping amount. The Mn−Mn distance for each composition is also plotted, revealing a simple linear relationship with x.

The relationship between the paramagnetic Curie temperature and the Mn−Mn distance of the $A_{14}MnPn_{11}$ (A = alkaline earth metals, Pn = Sb, Bi) compounds has been parametrized using the simple free electron isotropic RKKY theory.[4] The paramagnetic Curie temperature of the alkaline earth transition metal ternary analogues, which is related to the Mn−Mn coupling strength, increases smoothly as a function of decreasing Mn−Mn distance. The distance between two localized Mn moments is a key factor in determining the period and amplitude of the RKKY oscillation. However, in this rare earth transition metal pseudo-ternary solid solution system, the same relationship between the magnetic interaction strength and the distance of the Mn magnetic moments is no longer valid. The variation of the Mn−Mn distances in $Ca_{14-x}Eu_xMnSb_{11}$ is very small compared to those of the alkaline earth analogues. Therefore, the relatively wide and oscillating change of the paramagnetic Curie temperature of the solid solution should be considered as a function of the Eu concentration and site preference in the system.

The experimental results can be separated into three different regions for discussion and analysis. First, the sharp decrease of the paramagnetic Curie temperature, as x ranges from 0 to 2, is attributed to a disordering effect or the addition of frustration in the RKKY-type Mn−Mn magnetic interactions caused by the small amount of Eu doping. The slope of paramagnetic Curie temperature as a function of Mn−Mn distance is much sharper than that observed for the alkaline earth compounds. Therefore, in this low-x region, the paramagnetic Curie temperature cannot be modeled by the Mn−Mn distance alone. The preferential replacement of the Ca sites surrounding the Mn atom by Eu produces not only structural disorder but also perturbations in the conduction electron polarization. As a result, it appears that the coherence between the Friedel oscillations in the RKKY interaction is destroyed as a result of the Eu substitution, which subsequently decreases the Mn−Mn interaction strength and the paramagnetic Curie temperature in the regime $0 < x < 2$. The disordering effect (or frustration) on the medium of the RKKY interaction caused by chemical substitution has been studied in recent years.[26−28] The changes in the amplitude and period of the RKKY oscillation have exhibited a negative influence on the magnetic interaction due to the reduced symmetry. To verify our interpretation of the disordering effect in this first region of the solid solution, a new doping study of $Ca_{14-x}Yb_xMnSb_{11}$, in which we can consider the structural disorder only, will be performed.

In the next region of the solid solution, where x increases to 12, the paramagnetic Curie temperature increases as a function of increasing x. This arises from the contribution of R−T exchange interactions between $Eu^{2+}(4f^7)$ and $Mn^{3+}(3d^4)$, as discussed above. The enhanced magnetic interaction between Mn atoms is presumably established with the help of surrounding Eu local 4f moments via intra-atomic Eu 4f−5d polarization and subsequently an interatomic Mn,3d−Eu,5d exchange interaction.[25] It is noteworthy that the minimum paramagnetic Curie temperature in the solid solution shown in Figure 7 is approximately at the same composition as the 50% occupation of Eu in the Ca(2) site provided in Table 2. Eu substitution into the Ca(2) site contributes positively to the increase in Mn−Mn interaction strength after 50% substitution occurs. Ca(2) is the metal site closest to the Mn atom in this crystal structure. Thus, it is not surprising that the magnetic behaviors of the solid solution are governed by the amount of substitution of Eu into the Ca(2) site.

The slope change in the paramagnetic Curie temperature at $x = 12$ shown in Figure 7 was explained in the previous doping study[2] of the $Eu_{14}MnSb_{11}$ compound. In this region, the increase of the Eu substitution (~5%) into the Ca(2) site is much less than that into the other three Ca sites, particularly compared to the 21% for the Ca(3) site ($Ca_{1.5}Eu_{12.5}MnSb_{11}$, as shown in Table 2). The Ca(1) and Ca(3) sites frustrate the rest of the spins, thus, the magnetic interaction strength and the paramagnetic Curie temperature are decreased by the addition of more Eu spins in these sites.

(26) Ludoph, B.; Süllow, S.; Becker, B.; Nieuwenjuys, G. J.; Menovsky, A. A.; Mydosh, J. A. *Physica B* **1996**, *223/224*, 351−353.
(27) Kudrnovský, J.; Drchal, V.; Turek, I.; Sob, M.; Weinberger, P. *J. Magn. Magn. Mater.* **1996**, *156*, 245−246.
(28) Dietl, T.; Cibert, J.; Ferrand, D.; d'Aubigné, Y. M. *Mater. Sci. Eng.* **1999**, *B63*, 103−110.

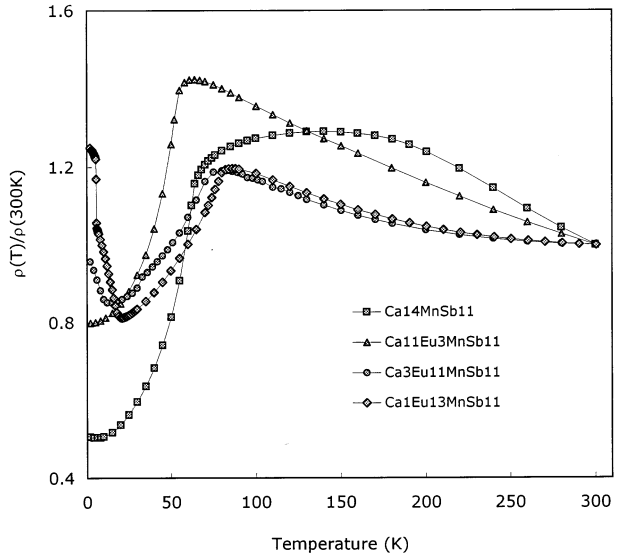

Figure 8. Four-probe electrical resistivities versus temperature for single-crystal samples of $Ca_{14-x}Eu_xMnSb_{11}$.

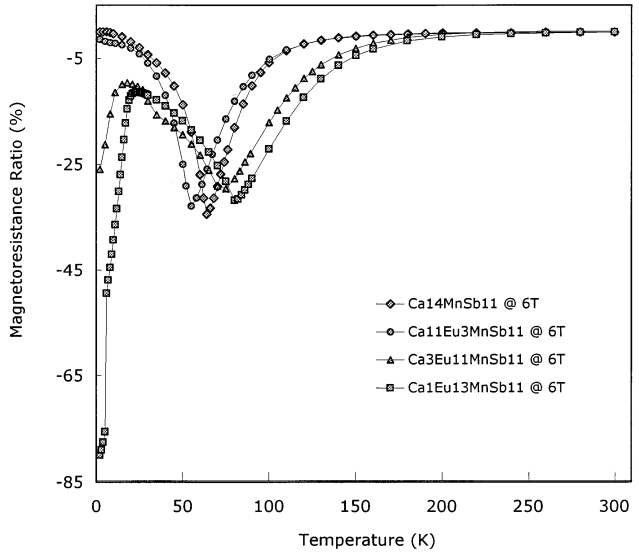

Figure 9. Magnetoresistance ratio versus temperature for single-crystal samples of $Ca_{14-x}Eu_xMnSb_{11}$.

Magnetoresistance. Figure 8 shows normalized resistivities of single-crystal samples of $Ca_{14-x}Eu_xMnSb_{11}$ ($x = 0, 3, 11, 13$) as a function of temperature. Each compound has the same transition from a high-temperature paramagnetic semiconducting state to a low-temperature ferromagnetic metallic state. The trend of the transition temperature change determined from the resistivity curves is consistent with the paramagnetic Curie temperature change from the magnetic measurement. The semiconductor-to-metal transition is closely related to the ferromagnetic ordering of the solid solution. There is another slope change at low temperature in the Eu-rich region ($x \geq 11$) of the solid solution, corresponding to the antiferromagnetic ordering of those compounds. The close relationship between magnetic and electronic properties suggests a significant contribution of spin scattering of conduction electrons caused by the localized magnetic ions.

Figure 9 shows a plot of the magnetoresistance ratio ($MR = [(\rho(6\ T) - \rho(0))/\rho(6\ T)] \times 100\%$) of the solid solution as a function of temperature. The large negative magnetoresistance effects of each compound are developed by the shift of magnetic transition to higher temperature caused by the applied magnetic field, and they are similar in magnitude to those of $Eu_{14}MnSb_{11}$.[29] The maximum MR value (approximately −80%) of $CaEu_{13}MnSb_{11}$[2] at the lowest temperature, 2 K, was attributed to its additional low-temperature transition below 6 K in the low magnetic field, which has been found in the single-crystal samples of the Eu-rich phases.

The origin of the colossal magnetoresistance (CMR) effect near the first magnetic transition temperature in the $A_{14}MnPn_{11}$ family was discussed in previous studies.[16,29−31] The CMR effect can be understood as a spin-scattering model of spin-polarized conduction electrons with the localized magnetic ions. The applied magnetic field will align the direction of localized magnetic spins, and conduction electrons will experience less spin scattering from the magnetic ordering. This study is also consistent with the model of conduction electrons from the Mn 4s band and s−d interactions based on the RKKY-type exchange causing the CMR effect. The similar order of the MR ratios of the solid solutions verifies that the Eu substitutions and their site preference for the various Ca sites does not have a large effect on the band structure of the solid solution. As concluded in the previous doping studies, the Eu 4f states need to be treated as spatially localized core states because the states do not hybridize with the valence band in the usual band structure theory.[32]

The CMR effect for this family of compounds is quite different than that for $Tl_{2-x}Sc_xMn_2O_7$ pyrochlore compounds,[33] where the Sc doping enhances the MR effect of the doped compound significantly by controlling electronic conduction on the thallium−oxygen sublattice without changing T_C. However, in the case of the $A_{14}MnPn_{11}$ family, the CMR effect is inevitably related to Mn metal, because both the electronic and magnetic properties of the compound are governed by the transition metal. The magnetotransport properties of this family of compounds are determined by the field dependence of T_C, which originates from the RKKY-type magnetic interaction between the Mn atoms. Another way to achieve enhancement of the CMR effect might be by changing the d-electron density, which might trigger a much higher magnetic field dependence of the transition temperature via modification of 3d−3d magnetic interaction and s−d spin scattering.

Acknowledgment. We thank the National Science Foundation (DMR 9803074) for funding. We thank R. N. Shelton for use of the SQUID magnetometer. The Bruker SMART 1000 diffractometer was funded in part by NSF Instrumentation Grant CHE-9808259.

Supporting Information Available: Crystallographic information for the compounds $Ca_5Eu_3MnSb_{11}$, $Ca_7Eu_7MnSb_{11}$, $Ca_9Eu_5MnSb_{11}$, $Ca_{11}Cu_3MnSb_{11}$, and $Ca_{13}Eu_1MnSb_{11}$ is available as cif formatted files. This material is available free of charge via the Internet at http://pubs.acs.org.

CM020065W

(29) Chan, J. Y.; Kauzlarich, S. M.; Klavins, P.; Shelton, R. N.; Webb, D. J. *Chem. Mater.* **1997**, *9*, 3132−3135.
(30) Chan, J. Y.; Kauzlarich, S. M.; Klavins, P.; Shelton, R. N.; Webb, D. J. *Phys. Rev. B* **1998**, *57*, R8103−R8106.
(31) Webb, D. J.; Cohen, R.; Klavins, P.; Shelton, R. N.; Chan, J. Y.; Kauzlarich, S. M. *J. App. Phys.* **1998**, *83*, 7192−7194.
(32) Richter, M. *J. Phys. D: Appl. Phys.* 1998, *31*, 1017−1048.
(33) Ramirez, A. P.; Subramanian, M. A. *Science* **1997**, *277*, 546−549.